Astron. Astrophys. 364, 712–722 (2000)

ASTRONOMY AND ASTROPHYSICS

Optical observations of the Draco molecular cloud

I. Catalog of B and V magnitudes for selected areas

B.E. Penprase[1], **J.D. Rhodes**[2], **and E.L. Harris**[1,⋆]

[1] Pomona College Department of Physics and Astronomy, 610 N. College Avenue, Claremont CA, USA (penprase@shanti.pomona.edu)
[2] Princeton University, Department of Physics, Princeton, N.J., USA (jrhodes@pupgg.princeton.edu)

Received 8 September 1997 / Accepted 17 July 2000

Abstract. To investigate the distance and linear dimensions of the Draco Molecular Cloud (MBM 41) we have obtained new CCD photometry for a selection of stars in 20 selected areas toward the cores of the cloud. The selected areas were chosen to coincide with the brightest IRAS emitting portions of the cloud, and also with dense ^{12}CO emission from the cloud. For each area we have obtained V and B photometry, and a subset of the fields has also been observed through a narrow-band Hα filter and in the U band.

We present V and B magnitudes for the 362 stars which have high-quality observations in both bands. In addition we have derived star counts in the V band using a larger sample of 465 stars, which is complete to a limiting magnitude of V=19.0. The star counts were compared to a galactic model from Bahcall & Soneira (1980). Using the galactic model of star counts, slightly modified to include the effects of a cloud of arbirary distance and extinction, we find a best fit to our data with values of A_V = 2.5 and $800 < d < 1300$ pc for the Draco molecular cloud. We also report results of photometric spectral classification using the index $[V-\alpha]$, which was found to correlate well with $(B-V)_0$ for our photometric standard stars. The modelled $B-V$ colors of the stellar sample were compared with the catalog values, and the observed colors best matched a cloud distance of d = 1100^{+200}_{-300} pc, with $A_V = 2.5 \pm 0.5$ and R_V = 1.5. Our photometry detects reddening and extinction from the densest portions of the Draco cloud, and it seems likely that the cloud is within the range of distances $800 < d < 1300$ pc, which corresponds to a height $|z|$ = 640 pc above the galactic plane, and linear dimensions as large as 40 pc for the cloud.

Key words: ISM: clouds – ISM: dust, extinction – ISM: general – ISM: structure – Galaxy: halo – techniques: photometric

1. Introduction

The Draco molecular cloud is one of the most interesting and enigmatic high galactic latitude molecular clouds known. It was first discovered from 21 cm observations, and was identified with an optical nebulosity in the Palomar Sky Survey (Goerigk et al. 1983). Additional observations in CO emission (Mebold et al. 1985), and more recent observations in soft X-rays with ROSAT (Herbstmeier et al. 1995) have given us greater knowledge of the cloud's composition, temperature, and kinematics, but the origin and distance to this cloud is still very uncertain. It appears as a compact and intricate "cometary cloud", approximately 5 degrees in extent, at galactic coordinates (l=90.0^o,b=38.0^o). The cloud is swept back into a number of dense clumps, and is surrounded by bright x-ray emission. The unusual appearance of the cloud, and its relatively large ^{12}CO velocity (v_{lsr} = -21 km s^{-1}) has led many authors to conclude that it may be a molecular cloud falling into our galaxy from either an extragalactic or 'galactic fountain' origin (Odenwald & Rickard 1987). In addition it has a strong X-ray shadow from ROSAT observations, and may be absorbing X-rays from beyond the local bubble (Burrows & Mendenhall 1991; Snowden et al. 1991)

The likely prospect that the Draco cloud is interacting with the halo of our galaxy near the edge of the X-ray emitting hot interstellar medium makes the determination of its distance very important for understanding the scale heights of both the neutral and hot components of the interstellar medium.

Mebold et al. (1985) attempted to derive a distance from star counts, and determined a distance of $300 < d < 800$ pc. A photometric study by Goerigk & Mebold (1986) increased the minimum possible distance to $d > 800$ pc, citing the lack of reddening in stars with $V < 14$. Lillenthal et al. (1991) attempted to detect the cloud from absorption lines of Na I D toward nearby bright stars, and derived a lower limit to the distance of $d > 180$ pc. More recently, Gladders et al. (1998) has derived a distance estimate of $463 < d < 618$ pc to the Draco cloud based on a single detection of Na I absorption from a background star.

In this work we present new CCD photometric observations of 362 stars with $14 \leq V \leq 19$ to provide a more complete sample of background stars which are expected to be at distances in excess of $d > 1200$ pc. By combining this photometry with star count models which include halo and disk populations of stars, an exponentially stratified H I background, and an intervening interstellar cloud of fixed distance and extinction we can constrain estimates of the distance and extinction of the Draco cloud.

Send offprint requests to: B.E. Penprase

⋆ Funded by a Hirsch Grant to B.E. Penprase

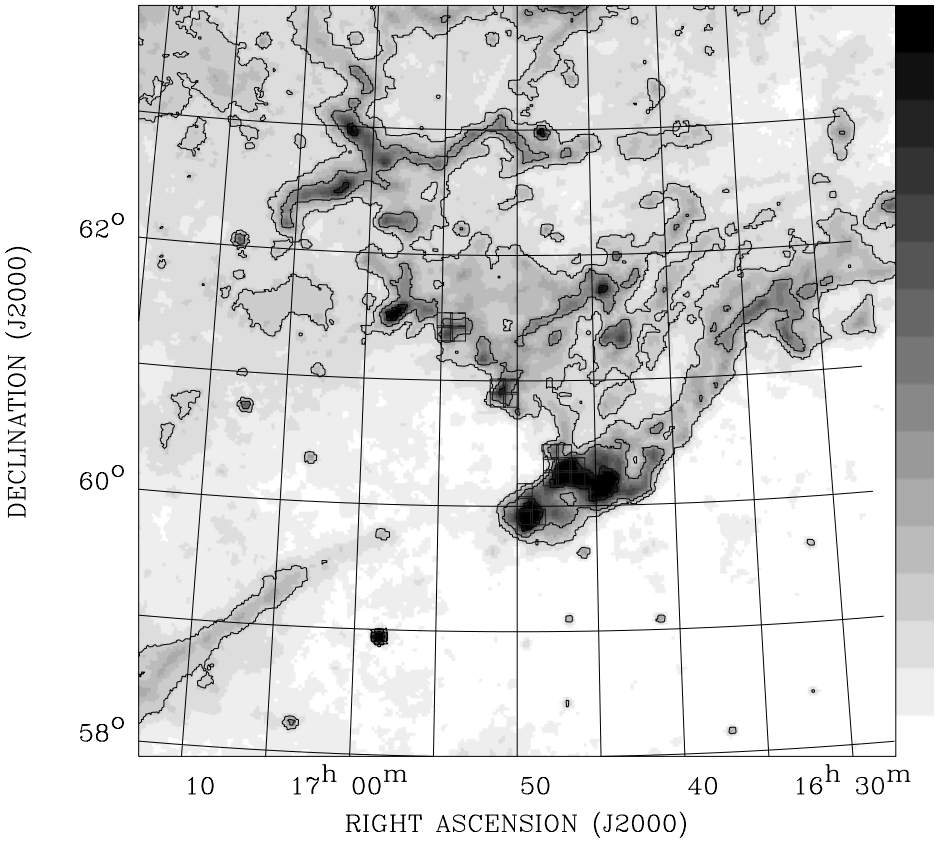

Fig. 1. IRAS 100μ image of the Draco Cloud, showing the wispy "cometary" nature of the cloud, and the selected areas for this work.

Examples of recent works which make use of similar techniques include Thoraval et al. (1997), who were able to model small scale structure in clouds using only star counts, and Andreazza et al. (1996) who report the extinction and structure of Southern dark clouds in Lupus and Corona Australius using star counts. Another study by Magnani & de Vries (1986) used digitized Palomar Sky Survey prints to derive distances to several high latitude cirrus clouds from an analysis of star counts. For our star count analysis we make use of the model of galactic structure from Bahcall & Soneira (1980), to which we have added an additional extinction term for an intervening molecular cloud at an arbitrary distance and extinction. This model was modified from the program 'galaxy' available on the internet, which was reviewed by Bahcall (1986). With this model and our new photometry, we hope to provide a solid basis for future studies of this fascinating object, and to give the first upper limits for the Draco cloud distance based on deep CCD photometry.

2. Observations

Our observations were taken during the nights of June 29 and June 30, 1993 at the Palomar Observatory, using the 1.5-meter telescope and Palomar 6 Tektronix CCD camera, using a 1024x1024 array with 24 micron pixels and low readout noise (8.2 e^-). The telescope and CCD provide a field of view of 6.3 arcminutes, with a plate scale of 15.48 arcsecs/mm. The limited field of view of the CCD allowed us to select fields which were contained exclusively within regions of the cloud which were bright in IRAS 100μm emission, as well as within regions of detectable emission in ^{12}CO. Our ^{12}CO maps were derived from the Bell Labs 10-meter telescope, and were kindly provided in advance of publication by Dr. Marc Pound. A view of the selected areas for our survey may be seen in Fig. 1, which presents an IRAS 100μm image from the ISSA survey (Wheelock et al. 1994), and the 20 selected areas indicated on the figure. The survey region concentrates on the Southern edge of the cloud, which is brightest and presumedly the densest portion of the cloud. Fig. 2 presents a more detailed view of the region studied, with the entire field shown from a mosaic of Digital Sky Survey plates, and the selected areas indicated. The coordinates and identifications for the selected area are presented below in Sect. 3.

CCD frames were taken for all of the 20 shown fields in the V and B filters during the first night, and a subset of these fields was observed during the second night in the U, V, B, and Hα filters. The filters used were multilayer custom U, B, and V filters designed by Dr. Jim Schombert of Caltech. The Hα filter was a 10 nm wide narrow-band filter centered at the rest wavelength of 6562 Å.

Each field was observed for at least 10 minutes in each of the filters, and duplicate frames were combined to improve the detectability of fainter stars. A summary of the observations is presented in Table 1. The fields were flat-fielded using dome flats and comic-ray and bias offsets were removed from the images. Instrumental magnitudes were obtained using the

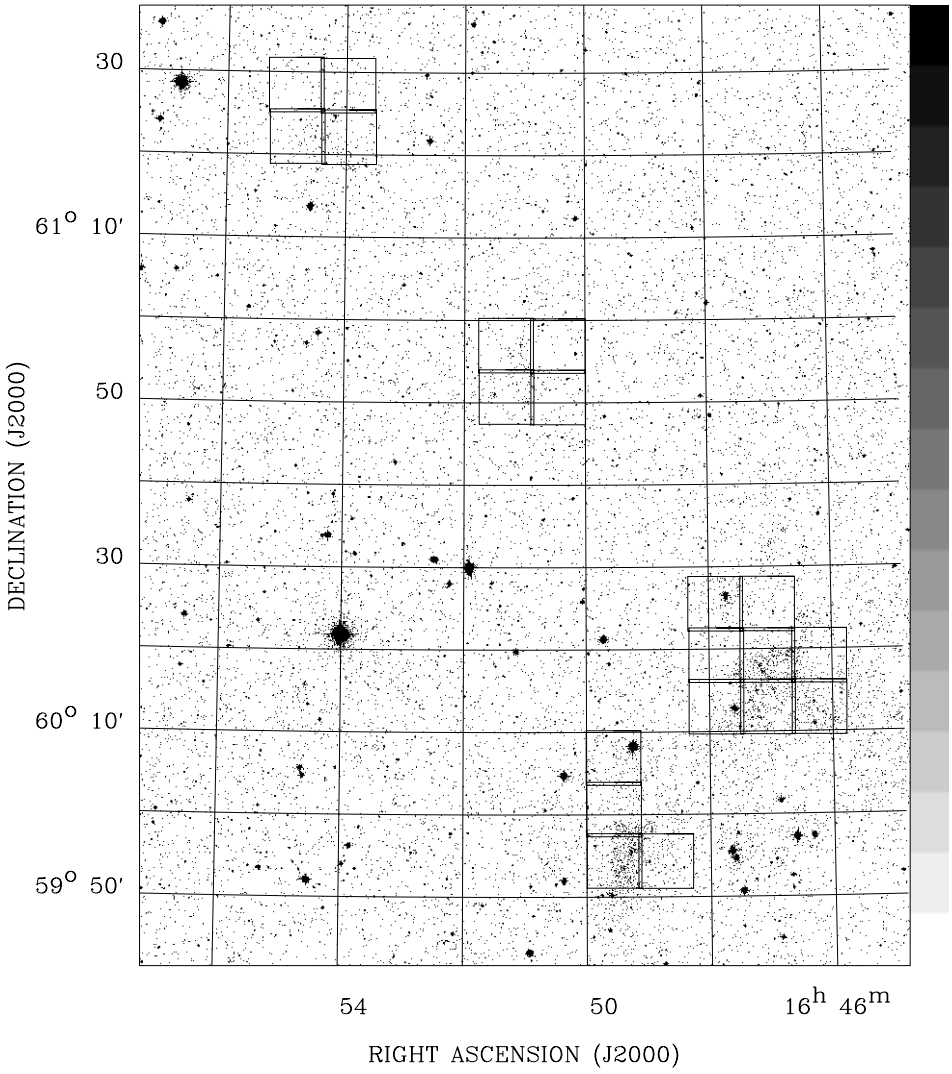

Fig. 2. Digital Sky Survey of the central Draco Cloud Region, showing in more detail the locations of our CCD fields observed with the Palomar Observatory 1.5-meter telescope

Table 1. Summary of observations

Night	N(stars)	N(fields)	Filt.	Exp.
1	465	20	V	600 s
1	362[1]	20	B	600 s
2	75	7	$H\alpha$	600 s
2	75	7	U	1200 s
2	75[2]	7	B	600 s
2	75[2]	7	V	600 s

[1] These 362 stars with good B and V photometry form the basis of the catalog in Appendix A. The 465 stars with V magnitudes were used for star-count analysis.
[2] These 75 stars with detectable U, Hα, B and V flux form the basis of Appendix B.

DAOFIND and DAOPHOT routines in IRAF, after carefully adjusting aperture sizes and testing background subtraction algorithms. Table 2 summarizes the fields studied. The 20 selected areas were chosen for their proximity to the dense cores in the Draco cloud, and were arranged in a grid of pointings spaced by the CCD field of view, and centered on the position at $16^h45^m30.24^s, +60^o18'07.56$" where radio maps indicate the peak of CO emission from the Draco Cloud. The arrangements of the CCD fields is shown in Fig. 2, which includes a digitized POSS image of the region near the Draco Cloud.

During the first night observations CCD photometric standard stars from Landolt (1992) were observed frequently at various airmasses to allow for removal of extinction and to derive transformation coefficients for converting the instrumental magnitudes into the standard Johnson B and V colors. Extinction corrections were performed using the standard star PG1525+071 observed at three different airmasses, and a linear least squares fit to the instrumental magnitudes indicated that the extinction correction for the range of airmass in our observations is δV < 0.1 magnitudes.

A total of 47 separate standard star observations during the first night were used to perform a linear least squares fit between instrumental and Johnson V and B magnitudes. The transformation coefficients are defined by:

$$V = v + \epsilon(B - V) + C_V \quad (1)$$

Table 2. Coordinates of selected area CCD fields

$FieldNo.$	$\alpha(1950)$	$\delta(1950)$
1	$16^h45^m30.24^s$	$+60^o18'07.56$"
2	$16^h45^m30.24^s$	$+60^o24'22.32$"
3	$16^h46^m20.64^s$	$+60^o18'07.56$"
4	$16^h46^m21.00^s$	$+60^o24'22.32$"
5	$16^h46^m21.00^s$	$+60^o30'37.44$"
6	$16^h47^m11.04^s$	$+60^o18'07.56$"
7	$16^h47^m11.10^s$	$+60^o24'22.32$"
8	$16^h47^m12.12^s$	$+60^o30'37.44$"
9	$16^h48^m00.00^s$	$+59^o59'22.56$"
10	$16^h48^m51.48^s$	$+60^o11'52.44$"
11	$16^h48^m50.76^s$	$+60^o05'37.68$"
12	$16^h48^m50.04^s$	$+59^o59'22.56$"
13	$16^h49^m48.00^s$	$+60^o55'37.56$"
14	$16^h49^m48.72^s$	$+61^o01'52.32$"
15	$16^h50^m39.48^s$	$+60^o55'37.56$"
16	$16^h50^m40.56^s$	$+61^o01'52.32$"
17	$16^h53^m21.84^s$	$+61^o26'52.44$"
18	$16^h53^m23.64^s$	$+61^o33'07.56$"
19	$16^h54^m14.04^s$	$+61^o26'52.44$"
20	$16^h54^m16.20^s$	$+61^o33'07.56$"

Table 3. Transformation coefficients for BV photometry

$Night$	ϵ	C_V	μ	C_{B-V}
1	0.08(.026)	3.74(.035)	0.96(.038)	−0.13(.037)
2	0.12(.029)	3.70(.040)	1.00(.050)	0.11(.050)

[a] Uncertainties indicated in parentheses

$$B - V = \mu(b - v) + C_{B-V} \quad (2)$$

where small letters indicate instrumental magnitudes, and the transformation coefficients ϵ,μ,C_V, and C_{B-V} are presented in Table 3. The transformation to the standard system appears accurate for our standard stars to within 0.1 magnitudes over the range of values of -0.25 $< B - V <$ 2.5.

A total of 465 stars were measured in V for the first night, and these stars were used for the star-count analysis of Sect. 3. A slightly smaller sample of 362 stars had good photometry in the B band, and V and $B-V$ magnitudes are presented for this sample in Appendix A. A histogram of V magnitudes for the 362 stars of the catalog (solid line), and the 465 stars with V magnitudes (dashed line) is presented in Fig. 3a, while a similar histogram of $B-V$ magnitudes of the 362 stars in our catalog is presented in Fig. 3b.

During the second night, we observed a subset of stars in all four passbands U, B, V, and Hα. The quantum efficiency for the CCD was too low to allow for useful determination of $U-B$ for all of the stars, so we extracted magnitudes in U, V, B, and $H\alpha$ for the 75 stars in 7 fields which had detectable U magnitudes. The results for these stars are presented in Appendix 2, and 35 of these stars were included in the larger catalog of Appendix 1.

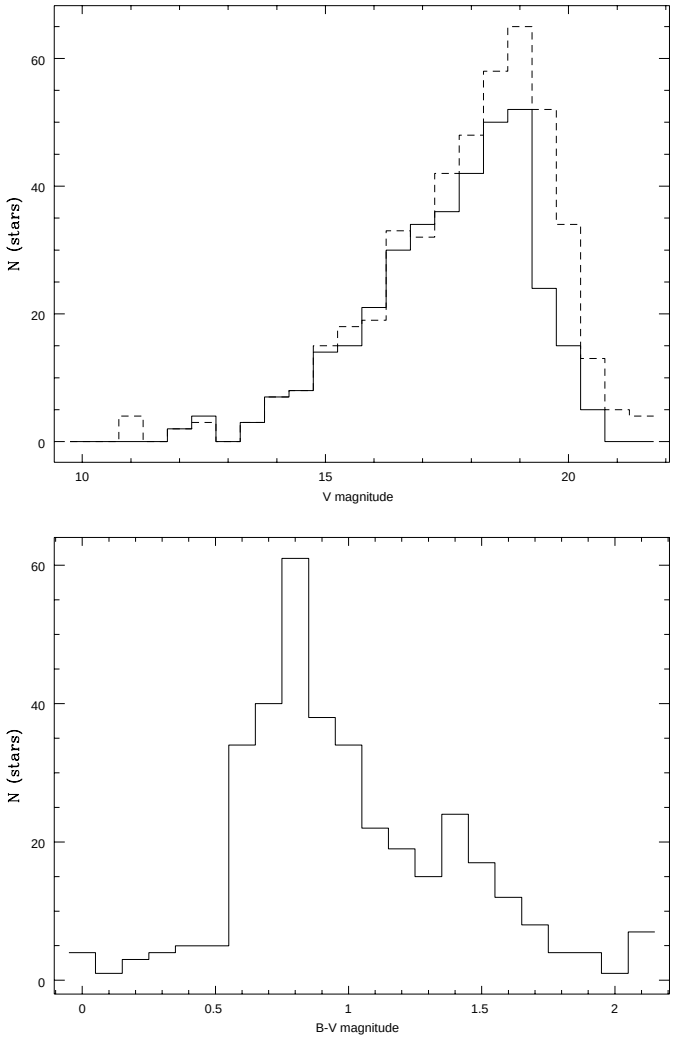

Fig. 3. (above) Histogram of the V magnitudes for the 362 stars of the catalog in Appendix A (solid line), and the 465 stars with V magnitudes (dashed line). (below) Histogram of the $B-V$ magnitudes for the catalog.

Fig. 4 shows a comparison between V magnitudes between the two nights, using the transformation coefficients in Table 3. The two nights agree to well within the uncertainty of 0.1 magnitudes, although there appears to be a systematic offset between the two nights of 0.04 magnitudes in V. We believe that the systematic error arises from the night 2 photometry, which had fewer standard star observations than the night 1 photometry.

Fig. 5 shows a comparison between $B-V$ colors between the two nights, using the transformation coefficients in Table 3. The two nights again agree to within the uncertainty of 0.1 magnitudes, with a similar small systematic offset between the two nights of 0.04 magnitudes.

In addition to the standard V and $B-V$ magnitudes, we have derived an index $[V-\alpha]$ which combines the observations at Hα with the V magnitude. The Hα counts for each star were converted to instrumental magnitudes, and for simplicity we used the same transformation constant C_V for getting the α magnitude. The $[V-\alpha]$ index was observed as a possible basis

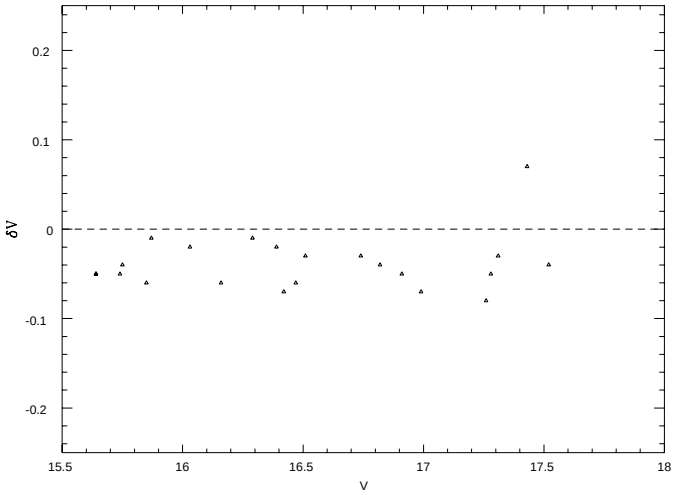

Fig. 4. Comparison between V values derived from the two nights of photometry, using the sample of stars common to both nights with detectable U fluxes. With the exception of a systematic offset of 0.04 magnitudes, the two nights agree to well within the stated photometric uncertainty of 0.1 magnitudes.

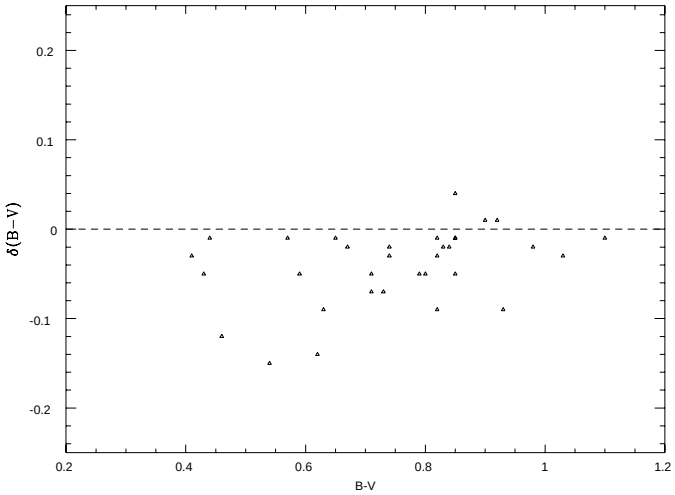

Fig. 5. Comparison of $B-V$ colors derived from the two nights of photometry, using the stars common to both nights with detectable U fluxes. Again, a systematic offset of 0.04 magnitudes is seen, but the photometry is consistent within the estimated uncertainty of 0.1 magnitudes.

for photometric classification, and can be used to detect chromospherically active stars (Grebel et al. 1992). We also discuss the effects of reddening on the $[V-\alpha]$ index and its possible use for photometric spectral classification in Sect. 3.3.

3. Results

3.1. Photometric catalog of V and $B-V$ for stars toward the Draco cloud

The results of the CCD photometry are presented below in Appendix A and B for nights 1 and 2, respectively. Appendix A presents coordinates of the stars and the V and $B-V$ magnitudes from the night 1 photometry. All the coordinates in Appendix A have been checked against the Digital Sky Survey Images, and we have found that the accuracy of the coordinates is typically 3 arcseconds or better. This catalog contains 362 stars which appear toward the densest part of the Draco Cloud, in the selected areas indicated in Fig. 1 and Fig. 2.

The photometry for the second night includes values of V, $B-V$, and $[V-\alpha]$, for the subset sample of 75 stars, and is presented in Appendix B. Many stars in Appendix B were not included in Appendix A, since the field centers of the second night did not coincide exactly with those of the first night. The stars in Appendix B were selected to have good quality U,α, as well as B and V observations. Appendix B presents a comparison of the photometry between the two nights for V and $B-V$, and coordinates of these 75 stars as measured against the field centers of the second night's data. The stars in Appendix B may include a mixture of early-type stars, and late-type stars with active chromospheres, as they were selected for high flux in U, B and Hα. Further spectroscopic work is underway to test this possibility.

Table 4. Line of sight distance for V=18

$Sp.Type$	M_V	$d_{E(B-V)=0}$	$d_{E(B-V)=0.25}$
$A5$	1.9	16600	11600
$F5$	3.3	8700	6100
$G5$	5.2	3630	2540
$K5$	7.3	1380	960
$M5$	12.8	110	80

[a] Distances based on M_V values from Mihalas & Binney (1981).

3.2. Photometric determination of the Draco cloud distance

We have attempted to derive the distance to the Draco Cloud using just the photometric observations, based on the assumption that the sample is deep enough to probe to very large distances. To give an overview of the depth of our program stars, Table 4 presents the expected line of sight distances for several main sequence stars of different spectral types, at a magnitude of V=18, and at two representative values of $E(B-V)$ for the foreground of the Draco Cloud.

It is clear from Table 4 that the magnitude limit of our sample, V=19, should be more than adequate to detect the Draco Nebula in absorption. In the following sections we present results that estimate the distance to the cloud using two methods. Sect. 3.3 presents the results of our tests of photometric classification of our program stars using a calibration of the index $[V-\alpha]$ to estimate $(B-V)_0$. Sect. 3.4 presents models of the counts in V magnitudes of the sample using a simulation of star numbers in the galaxy which includes realistic treatments of stellar populations, and stratification with $|z|$. Sect. 3.5 presents models of the expected color distributions of $B-V$ resulting front the same model, which is capable of constraining both the distance to the cloud, and the ratio of total to selective extinc-

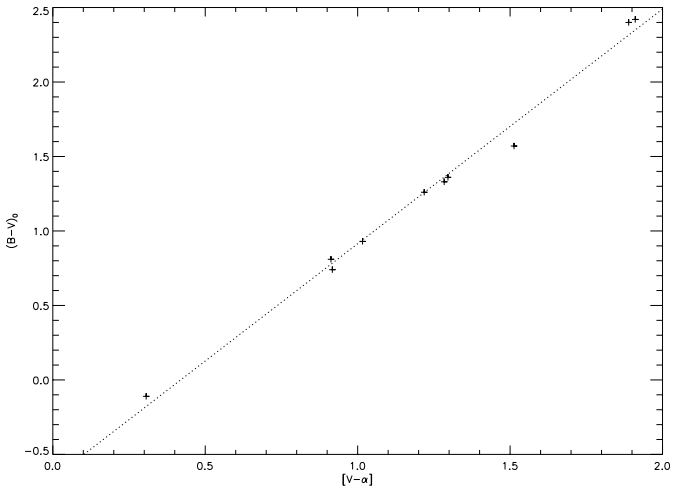

Fig. 6. Calibration of the photometric index $[V-\alpha]$ against the known values of $(B-V)_0$ for the 10 standard stars with MK spectral types from the second night.

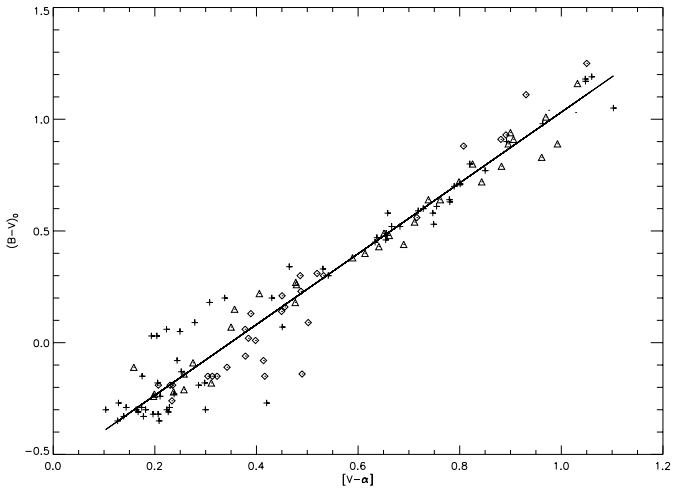

Fig. 7. Calibration of the synthetic photometry indices $[V-\alpha]$ against the known values of $(B-V)_0$ for 122 stars with unreddened digital spectra in the atlas of Jacoby et al. (1984). The luminosity class of the star is encoded by the plot symbol: crosses indicate class V, triangles indicate class III, and diamonds indicate class I. The slope of the relation for the stars was found to be m_{calib} = 1.584, in excellent agreement with the calibration photometry of our standard stars.

tion, R_V. With the combination of methods we have detected the extinction arising from the Draco cloud. This gives a basis for a preliminary distance estimate, and by comparing the methods, we can derive and estimate for the uncertainty in this estimate.

3.3. The $[V-\alpha]$ index and photometric spectral classification

The narrow-band Hα flux will depend strongly on MK spectral type for stars due to the decreasing Balmer hydrodgen line strengths for spectral types O-B-A, and less so for stars later than F. As such the index $[V-\alpha]$ could potentially be a useful tool for photometric spectral classification. The $[V-\alpha]$ index has been used previously to photometrically detect Be stars (Grebel et al. 1992) and was shown to be strongly correlated with $b-y$, and highly sensitive to chromospheric activity. If a calibrated dependence between $[V-\alpha]$ and $(B-V)_0$ can be shown for chromospherically inactive stars it is possible in principle to use just the measured values of $B-V$ and $[V-\alpha]$ to derive values of $(B-V)_0$ after correcting for the effects of reddening. We have performed a few experiments to test the feasibility of this technique for determining the distances to the stars in our sample.

To check the dependence between $[V-\alpha]$ and $(B-V)_0$ we used the ten Landolt standard stars observed in the second night, which were assumed to be unreddened. Fig. 6 shows a plot of the very strong linear relation between $[V-\alpha]$ and $(B-V)_0$ for these stars, which sampled a wide range of spectral types. The best fit line between these two indices corresponded to $(B-V)_0$ = 1.5753 $\times$ $[V-\alpha]$ - 0.6607. We believe that these bright standard stars in our sample are unreddened and free from chromospheric activity, but must acknowledge that either effect would disrupt our calibration. We have performed some analysis of the effects of lumunosity class, using a library of stellar spectra, and an analysis of the $[V-\alpha]$ index with synthetic photometry. No significant differences in the $[V-\alpha]$ index were found as a function of luminosity class, and the fitted slope to the data in Fig. 7 was found to be m_{calib}=1.584 $\pm$ 0.1, which is in excellent agreement with the calibration from our standard stars shown in Fig. 6.

While we believe that the calibration of $[V-\alpha]$ and $(B-V)_0$ has been determined for a sample of unreddened stars in the Figs. 6 and 7 above, a more difficult problem arises from the reddening of the $[V-\alpha]$ index. The $[V-\alpha]$ measurement is less susceptible to reddening than $B-V$, and using a standard extinction curve (Cardelli 1989), one predicts that for $E(B-V)$ = 0.1, the $[V-\alpha]$ index is reddened by a value of $E([V-\alpha])$ = 0.078. The result is a reddening vector in the $B-V$,$[V-\alpha]$ plane with a slope of m_{red} = 1.28, which is very close to the derived slope of m_{calib} = 1.58 in the $[V-\alpha]$ and $(B-V)_0$ calibration. It is therefore very difficult to apply the $[V-\alpha]$ index for photometric spectral classification without extremely accurate photometry to enable dereddening of the observed $B-V$,$[V-\alpha]$ colors. It is however possible in principle to solve for $E(B-V)$, using the observed $B-V$,$[V-\alpha]$ colors and the reddening vector.

While in some respects the $[V-\alpha]$ index may be useful for photometric spectral classiciation, we conclude that for the stars in the present work, the combination of photometric uncertainties and variations in reddening (along with the possibility of chromospheric activity in the stars) makes the $[V-\alpha]$ unreliable for determining $(B-V)_0$ and M_V. We have included this analysis to explore the applicability of this index for future photometric classification projects, where it may be useful for studying chromospherically inactive stars of uniform or little reddening. The $[V-\alpha]$ index could therefore be applied toward the photometric classification of early-type stars too faint for traditional $uvby$ or UBV photometry which are unreddened, or in a cluster of known reddening.

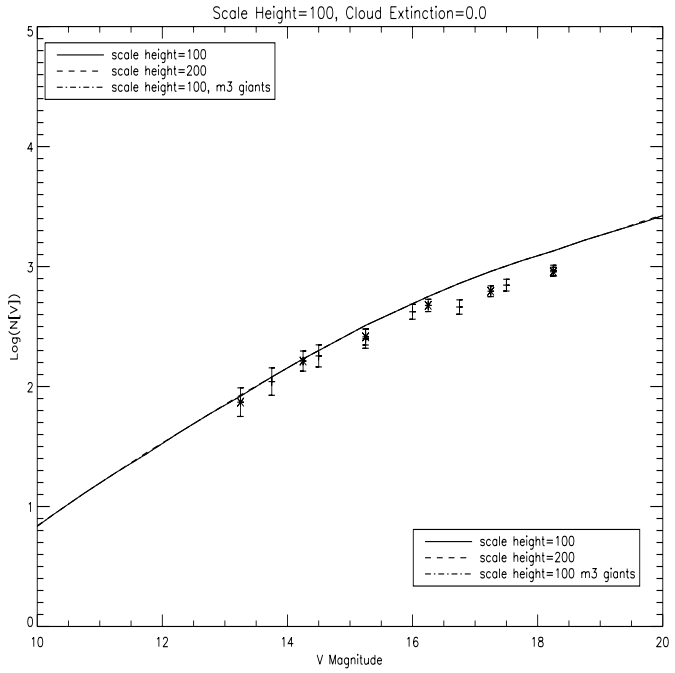

Fig. 8. Results of star-count models at the coordinates of the Draco nebula, to test the effects of varying the scale height of HI and the giant branch colors used in the simulation. These models do not include the effects of an intervening interstellar cloud and show that the models are insensitive to the effects of the other variables. Included in the plots are the measured star counts from our samples; the star counts and uncertainties are indicated on the plot for two different binnings of V magnitudes – 0.5 magnitudes (crosses) and 0.75 magnitudes (stars).

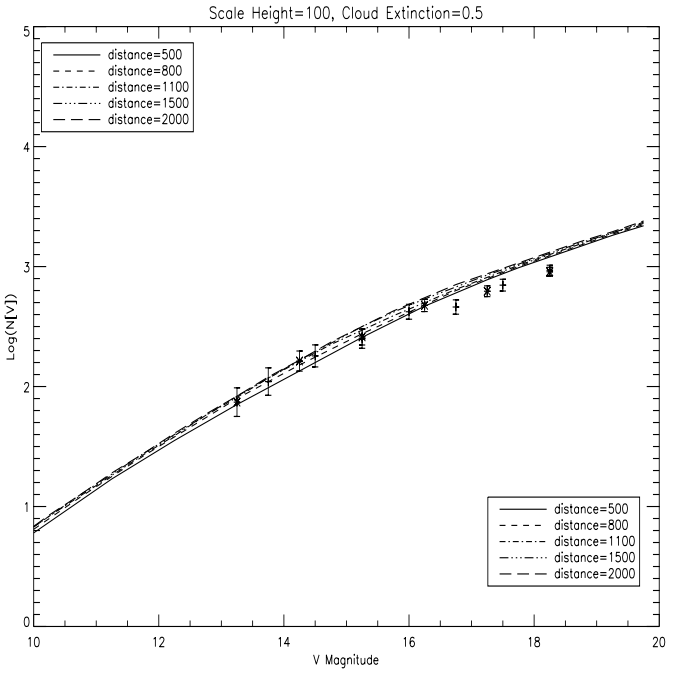

Fig. 9. Results of a star-count model, which includes the effects of an interstellar cloud at several distances ranging from distances of 500-2000 pc, and a total A_V of 0.5 magnitudes. The measured star counts and their uncertainties are indicated on the plot for two different binnings of V magnitudes – 0.5 magnitudes (crosses) and 0.75 magnitudes (stars).

3.4. Derivation of cloud extinction and distance from star count models

We have also used a model of the galaxy from Bahcall & Soneira (1980), which predicts observed star counts and colors at any galactic coordinates. We have modified this model to include the effects of a high latitude cloud, which is considered as a slab of gas at a given distance and extinction.

In our simulations we have included three populations of stars to model the galactic star counts at the galactic coordinates (l=90.0^o,b=38.7^o) near the center of the Draco nebula. We include stars from the disk, bulge and halo, with giant branch colors adopted from the globular cluster M13. Our models include an exponentially stratified HI layer of scale height $|z|$ = 100 pc. Further details on the model can be found in Bahcall & Soneira (1980). We then compute the effects on the star counts with the addition of an interstellar cloud as a function of cloud distance, extinction A_V, and total to selective extinction R_V. The modelled star counts were then compared with the observed star counts in our CCD fields.

Our CCD photometric sample for the star counts includes 465 stars with good V magnitudes, which is a superset of the stars included in Appendix A. The data in Fig. 8-12 include two binning modes in V magnitudes: a bin size of 0.5 in V (crosses) and bin size of 0.75 magnitudes in V (asterisks). Error bars for each bin were computed from the Poisson statistics of the sample size in each magnitude range. The smaller error bars for the 0.75 magnitude bins reflect the larger number of stars within each bin.

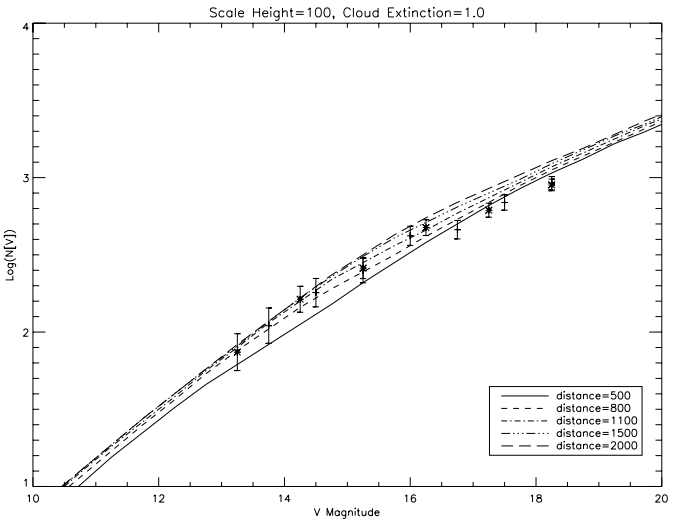

Fig. 10. Results of a star-count model, which includes the effects of a cloud at several distances ranging from distances of 500-2000 pc, and a total A_V of 1.0 magnitudes. The measured star counts and their uncertainties are indicated on the plot for two different binnings of V magnitudes – 0.5 magnitudes (crosses) and 0.75 magnitudes (stars).

In Fig. 8 we present the data from our star counts, and the modelled star counts without an intervening interstellar cloud,

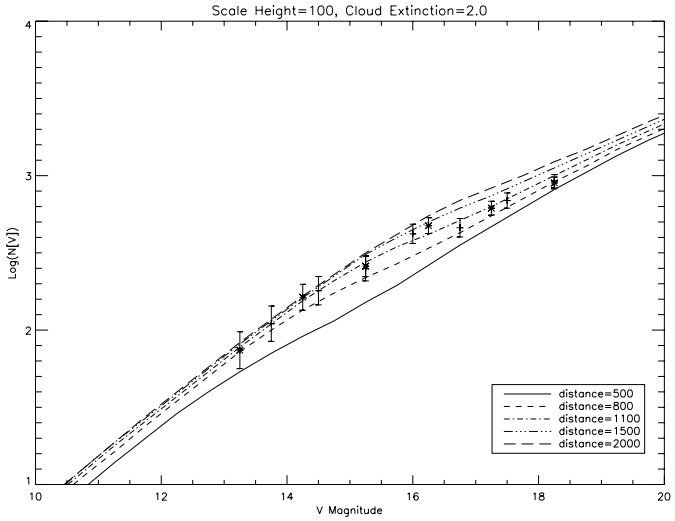

Fig. 11. Results of a star-count model, which includes the effects of a cloud at several distances ranging from distances of 500-2000 pc, and a total A_V of 2.0 magnitudes. The measured star counts and their uncertainties are indicated on the plot for two different binnings of V magnitudes.

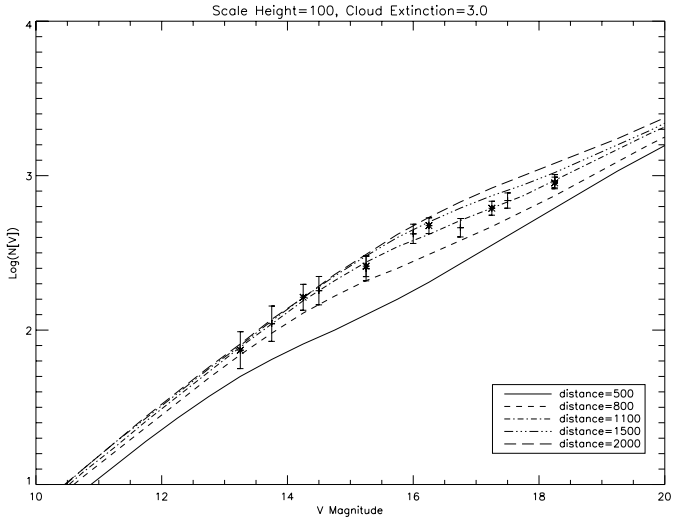

Fig. 12. Results of a star-count model, which includes the effects of a cloud at several distances ranging from distances of 500-2000 pc, and a total A_V of 3.0 magnitudes. The measured star counts and their uncertainties are indicated on the plot for two different binnings of V magnitudes.

while varying some of the other parameters in the model (scale height and giant branch colors). Fig. 8 shows that the star count models are insensitive to these parameters, and that the models do not match the data well without including the effects of the absorbing interstellar cloud.

Figs. 9, 10, 11 and 12 show models which include the expected star counts with an intervening interstellar cloud at a range of distances from $500 < \mathrm{d} < 2000$ pc, at values of cloud extinction A_V of 0.5, 1.0, 2.0, and 3.0 magnitudes, respectively.

It is possible to see from Figs. 8-12 that the effects of the cloud are detected in our star counts, and that the best fit models are found with clouds that have extinction in the range $1.0 < \mathrm{A}_V < 3.0$ and distances in the range of $800 < \mathrm{d} < 1500$ pc. Of all the models considered, our star-counts are most consistent with the values of $2.0 < \mathrm{A}_V < 3.0$ magnitudes, and d = 1100 pc. We have adopted the value of A_V=2.5 ± 0.5 magnitudes to indicate the range of values for which the star counts provide acceptable fits to within our estimated uncertainties.

3.5. Theoretical $B-V$ colors for stars and effects of distance, A_V and R_V

In addition to the counts of stars as a function of brightness, we also have modelled the theoretical colors of a sample of stars within this same region. Additional free parameters, such as the ratio of total to selective extinction, R_V, and the magnitude limit of our sample in the B passband, need to be evaluated in order to estimate the colors in the sample.

The colors of the sample of stars were derived using the same modified Bahcall and Soneira model, with the additional free parameter of R_V. A range of distances from $800 < \mathrm{d} < 2000$ pc was evaluated, over several values of extinction ranging from $1.0 < \mathrm{A}_V < 3.0$, and values of R_V ranging from $1.5 < \mathrm{R}_V < 9.0$.

The variation of any of these parameters was found to have a significant effect on the predicted $B-V$ colors, and for most values we tested, the colors predicted were bimodal, with a large peak in the histogram for values of $B-V \leq 0.9$, and a separate red peak for $B-V \geq 1.5$.

An examination of the observed $B-V$ colors of our sample seen in Fig. 3 and Fig. 13 shows a similar, less pronounced bimodal distribution of colors than predicted in the models. This may be caused by our selection of stars which have both detectable B and V magnitudes, which may remove several of the reddest stars in the sightline if our B limiting magnitude is (as expected) brighter than the V magnitude. For this reason, we have emphasized the modelled colors of the bluer stars in comparing with our observed $B-V$ distributions.

Suprisingly, only one set of the parameters d, A_V, and R_V matched the bluer peak in the color distribution well. We present in Fig. 13 a plot of a few of the models using the mean value of A_V = 2.5 derived from the star-count analysis. Fig. 13 shows the observed $B-V$ color histogram for the sample of Appendix A, and the modelled fit for A_V = 2.5 and the default R_V = 3.0 at the distance of d = 1100 pc. Additional lines in Fig. 13 show the modified fits using R_V = 1.5, at a range of distances from 800 to 2000 pc. With the exception of the large peak in the number of red stars in our model, good agreement in the colors is seen for the A_V=2.5 model with R_V = 1.5 and d = 1100 pc.

4. Conclusions

From our CCD photometric observations, we believe that we have convincingly detected evidence of extinction from the Draco cloud within our sample, and have some preliminary basis for estimating the distance to this object. In addition, our photometric catalog of stars is large and deep enough that we

Table 5. Appendix A: V and $B-V$ values and coordinates for the program stars[1]

Object	V	$B-V$	$R.A.(1950)$	$Dec(1950)$	*Object*	V	$B-V$	$R.A.(1950)$	$Dec(1950)$
$PRHB165335+612921$	11.85	0.64	$16^h53^m35.56^s$	$61^o29'21.10"$	$PRHB164931+610056$	11.96	0.93	$16^h49^m31.93^s$	$61^o0'56.25"$
$PRHB164757+602059$	12.37	0.69	$16^h46^m57.90^s$	$60^o20'59.86"$	$PRHB165410+612852$	12.39	0.72	$16^h54^m10.59^s$	$61^o28'52.66"$
$PRHB164909+600532$	12.55	1.05	$16^h49^m9.55^s$	$60^o5'32.57"$	$PRHB164648+601548$	12.71	0.78	$16^h46^m48.53^s$	$60^o15'48.30"$
$PRHB164816+595915$	13.29	0.66	$16^h48^m16.47^s$	$59^o59'15.71"$	$PRHB164615+602944$	13.35	1.06	$16^h46^m15.88^s$	$60^o29'44.85"$
$PRHB164636+601650$	13.58	1.11	$16^h46^m36.63^s$	$60^o16'50.64"$	$PRHB164940+605750$	13.79	1.33	$16^h49^m40.34^s$	$60^o57'50.00"$
$PRHB164649+602032$	13.82	0.76	$16^h46^m49.24^s$	$60^o20'32.45"$	$PRHB164958+601438$	14.01	0.67	$16^h48^m58.97^s$	$60^o14'38.47"$
$PRHB164926+605638$	14.02	0.61	$16^h49^m26.89^s$	$60^o56'38.52"$	$PRHB164852+601220$	14.05	0.73	$16^h48^m52.09^s$	$60^o12'20.09"$
$PRHB165051+605551$	14.12	0.84	$16^h50^m51.18^s$	$60^o55'51.68"$	$PRHB165023+610500$	14.17	0.88	$16^h50^m23.19^s$	$61^o5'0.95"$
$PRHB165350+612530$	14.28	0.62	$16^h53^m50.94^s$	$61^o25'30.57"$	$PRHB165004+610423$	14.42	0.64	$16^h50^m4.65^s$	$61^o4'23.94"$
$PRHB165004+610345$	14.43	0.79	$16^h50^m4.40^s$	$61^o3'45.46"$	$PRHB164716+601923$	14.44	0.66	$16^h47^m16.30^s$	$60^o19'23.23"$

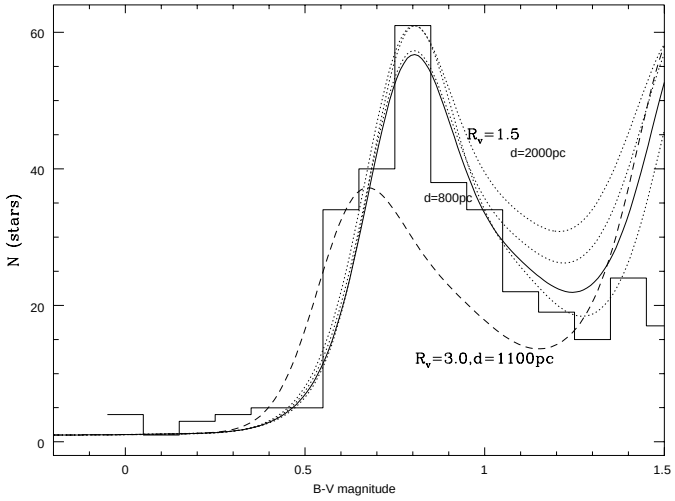

Fig. 13. Modelled $B-V$ colors for the sample using A_V, superimposed on the observed colors from the Appendix A, for a fixed cloud extinction A_V=2.5, and a range of values of cloud distance and R_V. The default value of R_V=3.0 was unable to duplicate the observed $B-V$ colors (dashed line). The best fit is seen for d=1100 pc, A_V=2.5, and R_V=1.5 (solid line). The lack of a large number of observed stars at $B-V > 1.5$ probably results from a brighter limiting magnitude in B than in V, which would prevent inclusion of many of the faint, redder stars predicted in the model.

should have several included stars which are in the background of the cloud.

This work forms a basis for further observational studies of the Draco nebula, using more accurate spectroscopic and polarimetric techniques upon the stars in our catalog to constrain the distance and other properties of the cloud. We may summarize the results of this work below.

1. We have presented a photometric catalog which includes sufficient depth (V > 19) to detect the Draco nebula if it is a galactic object.
2. A strong correlation between the photometric index $[V-\alpha]$ and $(B-V)_0$ is found for our standard stars.
3. The use of the photometric index $[V-\alpha]$ is a possible technique for photometric classification of faint, unreddened, chromospherically inactive early-type stars for which $uvby$ photometry may be difficult, but high precision photometry and/or a reddening free index may be needed to accurately calculate the reddening toward the sightline.
4. Preliminary indications indicate that the Draco nebula is detected from photometric reddening of our sample, with a best fit distance of d=1100^{+200}_{-300} pc, and extinction A_V=2.5 ± 0.5 magnitudes.
5. The predicted $B-V$ colors from our star count models are most consistent with a sample of stars with a limiting V magnitude of V=19 and a brighter B limiting magnitude of B = 18, which detects absorption from the Draco Nebula at a distance of 800 < d < 1100 pc, and with a cloud R_V = 1.5 ± 0.5, and extinction of A_V=2.5 magnitudes.
6. Our catalog of V, $B-V$, and $[V-\alpha]$ magnitudes for the Draco nebula should be a valuable tool for future spectroscopic and polarimetric studies of the cloud.

We also would like to note that with the above values of distance, R_V, and A_V, the Draco cloud is quite an exceptional object. The dense clumps in the cloud have angular sizes which range from 2 to 20 arcminutes, which correspond at d=1100 pc to linear dimensions of l=0.65 to 6.5 pc. Indeed the largest 'plumes' of this cometary cloud are close to 2 degrees across, which would correspond to a linear dimension of 38 pc at the adopted distance. This would make the Draco cloud a very large object indeed, more comparable in size to galactic plane giant molecular clouds than typical high latitude clouds, and at a scale height $|z|$ = 640 pc which is well above the typical scale height of 90 pc for molecular clouds in the galaxy.

Additional observations and theoretical work are clearly needed to provide more accurate constraints on the possible mass, origin and internal conditions of the Draco nebula, which

[1] Appendix A and B are also available in electronic form at the CDS via anonymous ftp to cdsarc.u-strasbg.fr (130.79.128.5) or via http://cdsweb.u-strasbg.fr/Abstract.html

Table 6. Appendix B: Stars with complete V, $B-V$, $U-B$, and $[V-\alpha]$ photometry, and comparison with night 1

Object	$V(n1)$	$B-V(n1)$	$V(n2)$	$B-V(n2)$	$U-B$	$[V-\alpha]$	$R.A.(1950)$	$Dec(1950)$
$PRHB164540+602042$	17.34	0.80	17.26	0.73	0.07	0.79	$16^h45^m39.84^s$	$+60^o20'43.36"$
$PRHB164510+602015$	...	...	17.83	0.66	0.27	1.07	$16^h45^m10.05^s$	$+60^o20'15.13"$
$PRHB164531+602012$	...	...	17.29	0.94	0.08	1.12	$16^h45^m31.11^s$	$+60^o20'12.58"$
$PRHB164508+601945$	...	...	14.31	0.76	0.33	0.95	$16^h45^m08.49^s$	$+60^o19'45.52"$
$PRHB164509+601831$	...	...	15.88	0.63	0.02	0.85	$16^h45^m09.35^s$	$+60^o18'31.57"$
$PRHB164507+601817$	...	...	15.41	0.62	0.11	0.91	$16^h45^m07.66^s$	$+60^o18'17.42"$
$PRHB164516+601758$	16.53	0.85	16.47	0.83	0.29	0.95	$16^h45^m15.93^s$	$+60^o17'58.74"$
$PRHB164532+601750$	15.31	1.00	15.27	0.98	0.79	1.13	$16^h45^m31.78^s$	$+60^o17'51.01"$
$PRHB164540+601703$	16.54	1.02	16.51	0.93	0.41	1.01	$16^h45^m39.62^s$	$+60^o17'03.58"$
$PRHB164518+601546$	16.91	1.75	17.88	0.87	1.48	0.94	$16^h45^m17.25^s$	$+60^o15'46.91"$
$PRHB164540+601522$	...	...	18.02	0.71	0.93	0.75	$16^h45^m40.55^s$	$+60^o15'22.93"$
$PRHB164543+602726$	16.49	0.85	16.42	0.80	0.24	1.01	$16^h45^m42.09^s$	$+60^o27'26.27"$
$PRHB164537+602713$	17.06	0.81	16.99	0.85	0.38	0.93	$16^h45^m36.22^s$	$+60^o27'13.20"$
$PRHB164517+602648$	14.50	0.76	14.44	0.74	0.28	0.97	$16^h45^m16.11^s$	$+60^o26'48.38"$
$PRHB164506+602603$	15.79	0.69	15.75	0.67	0.22	0.91	$16^h45^m05.53^s$	$+60^o26'03.16"$
$PRHB164631+602002$	...	...	12.28	0.61	-0.30	0.95	$16^h46^m31.39^s$	$+60^o20'02.95"$
$PRHB164611+601904$	...	...	18.47	0.48	-1.44	1.02	$16^h46^m11.61^s$	$+60^o19'04.88"$
$PRHB164638+601839$	...	...	16.19	0.86	0.33	1.03	$16^h46^m38.46^s$	$+60^o18'39.04"$
$PRHB164614+601807$	15.79	0.83	15.74	0.83	0.28	1.00	$16^h46^m12.35^s$	$+60^o18'07.12"$
$PRHB164607+601736$	...	...	18.22	0.68	0.54	1.12	$16^h46^m07.44^s$	$+60^o17'36.06"$
$PRHB164613+601715$	...	...	18.22	0.67	0.03	0.78	$16^h46^m13.01^s$	$+60^o17'15.44"$
$PRHB164636+601650$	13.58	1.11	13.54	1.10	0.95	1.21	$16^h46^m35.44^s$	$+60^o16'50.65"$
$PRHB164627+601647$	...	...	13.59	1.10	0.74	1.16	$16^h46^m27.10^s$	$+60^o16'47.65"$
$PRHB164620+601522$	14.46	0.86	14.43	0.84	0.60	1.00	$16^h46^m20.83^s$	$+60^o15'27.44"$
$PRHB164615+602720$	...	...	14.56	0.48	0.02	0.81	$16^h46^m15.33^s$	$+60^o27'20.01"$
$PRHB164622+602541$	...	...	16.52	0.70	0.26	0.87	$16^h46^m22.29^s$	$+60^o25'41.15"$
$PRHB164607+602445$	...	...	16.99	0.85	0.69	0.97	$16^h46^m07.04^s$	$+60^o24'45.54"$
$PRHB164601+602430$	...	...	15.39	0.94	0.37	1.09	$16^h46^m01.36^s$	$+60^o24'30.49"$
$PRHB164614+602419$	...	...	14.87	0.91	0.36	1.02	$16^h46^m14.43^s$	$+60^o24'19.36"$
$PRHB164634+602257$	...	...	17.03	0.82	-0.55	0.80	$16^h46^m34.07^s$	$+60^o22'57.90"$
$PRHB164555+602228$	...	...	16.65	1.02	0.72	1.18	$16^h45^m55.88^s$	$+60^o22'28.65"$
$PRHB164617+603342$	15.08	0.77	15.04	0.74	0.39	0.96	$16^h46^m16.37^s$	$+60^o33'37.99"$
$PRHB164604+603324$	15.69	0.58	15.64	0.57	0.12	0.82	$16^h46^m03.07^s$	$+60^o33'19.53"$
$PRHB164616+603154$	17.56	0.45	17.52	0.44	-0.29	-0.11	$16^h46^m14.96^s$	$+60^o31'49.93"$
$PRHB164640+603136$	16.96	0.86	16.91	0.85	0.45	1.03	$16^h46^m39.47^s$	$+60^o31'32.11"$
$PRHB164634+603055$	18.43	0.76	18.48	0.62	0.98	0.46	$16^h46^m33.22^s$	$+60^o30'50.79"$
$PRHB164615+602944$	13.35	1.06	13.31	1.03	0.88	1.09	$16^h46^m14.76^s$	$+60^o29'40.52"$
$PRHB164605+602943$	16.41	0.48	16.39	0.43	-0.24	0.68	$16^h46^m04.42^s$	$+60^o29'39.62"$
$PRHB164615+602924$	16.05	0.64	16.03	0.59	0.01	0.85	$16^h46^m14.77^s$	$+60^o29'20.08"$
$PRHB164638+602813$	16.30	0.78	16.29	0.71	0.32	0.92	$16^h46^m36.99^s$	$+60^o28'09.32"$
$PRHB164648+602126$	...	...	16.58	0.83	0.07	1.54	$16^h46^m48.13^s$	$+60^o21'26.43"$
$PRHB164657+602059$	12.37	0.69	12.52	0.54	-0.03	1.07	$16^h46^m56.72^s$	$+60^o20'57.29"$

challenges many of our ideas about the structure of the galactic interstellar medium.

Acknowledgements. This work was sponsored by a generous grant from the Hirsch family of Los Angeles, which supported Eirik Harris, provided travel money and computer resources for the project. Additional computational support was provided by a grant from the Mellon Foundation and the Pomona College physics and astronomy department. We also would like to thank John Bahcall of the Princeton Institute for Advanced Study for making the 'galaxy' program available over the internet. We would like to thank the referees, U. Mebold, and K. de Boer for many useful comments which greatly improved the paper. K. de Boer is also to be thanked for pointing out the effects of reddening and chromospheric activity on the $[V-\alpha]$ index.

Table 6. Appendix B: Stars with complete V, $B-V$, $U-B$, and $[V-\alpha]$ photometry, and comparison with night 1 (continued)

Object	$V(n1)$	$B-V(n1)$	$V(n2)$	$B-V(n2)$	$U-B$	$[V-\alpha]$	$R.A.(1950)$	$Dec(1950)$
$PRHB164648+602029$	...	...	13.78	0.75	0.38	0.94	$16^h46^m48.04^s$	$+60^o20'29.90"$
$PRHB164715+601945$	16.77	0.44	16.74	0.41	−0.05	0.56	$16^h47^m13.90^s$	$+60^o19'42.39"$
$PRHB164650+601935$	...	...	16.51	0.57	0.23	1.03	$16^h46^m50.73^s$	$+60^o19'35.48"$
$PRHB164716+601923$	14.44	0.66	14.39	0.65	0.21	0.88	$16^h47^m15.12^s$	$+60^o19'20.49"$
$PRHB164712+601805$	15.14	0.86	15.09	0.85	0.60	0.65	$16^h47^m11.47^s$	$+60^o18'03.07"$
$PRHB164647+601545$	...	...	12.77	0.68	0.44	1.06	$16^h46^m47.34^s$	$+60^o15'45.72"$
$PRHB164658+602651$	...	...	17.81	0.86	0.31	1.11	$16^h46^m58.59^s$	$+60^o26'51.10"$
$PRHB164729+602541$	...	...	15.16	0.60	0.11	0.87	$16^h47^m29.92^s$	$+60^o25'41.50"$
$PRHB164713+602530$	...	...	17.97	0.68	−0.03	1.11	$16^h47^m13.34^s$	$+60^o25'30.38"$
$PRHB164701+602529$	...	...	13.23	0.62	0.19	0.83	$16^h47^m01.70^s$	$+60^o25'29.21"$
$PRHB164708+602412$	...	...	15.85	0.61	0.02	0.84	$16^h47^m08.19^s$	$+60^o24'12.45"$
$PRHB164650+602317$	...	...	16.00	1.16	1.29	1.18	$16^h46^m50.68^s$	$+60^o23'17.57"$
$PRHB164720+602246$	...	...	16.22	0.51	−0.08	0.79	$16^h47^m20.82^s$	$+60^o22'46.54"$
$PRHB165016+610233$	...	...	14.62	0.70	0.32	0.93	$16^h50^m16.81^s$	$+61^o02'33.75"$
$PRHB165044+610258$	...	...	15.75	0.60	0.08	0.84	$16^h50^m44.92^s$	$+61^o01'58.97"$
$PRHB165044+610128$	...	...	18.08	0.46	−0.85	1.18	$16^h50^m44.12^s$	$+61^o01'28.97"$
$PRHB165035+610050$	...	...	15.05	0.79	0.18	0.97	$16^h50^m35.41^s$	$+61^o00'50.82"$
$PRHB165044+610002$	...	...	17.61	1.06	0.19	1.35	$16^h50^m44.66^s$	$+61^o00'02.75"$
$PRHB165349+613011$	16.86	0.84	16.82	0.79	0.26	1.01	$16^h53^m48.62^s$	$+61^o30'10.54"$
$PRHB165429+612902$	17.36	0.58	17.43	0.46	−0.17	0.85	$16^h54^m28.37^s$	$+61^o29'01.13"$
$PRHB165410+612852$	12.39	0.72	12.40	0.63	0.08	0.96	$16^h54^m09.41^s$	$+61^o28'51.64"$
$PRHB165423+612807$	17.33	0.76	17.28	0.71	−0.15	0.81	$16^h54^m21.82^s$	$+61^o28'06.42"$
$PRHB165355+612730$	15.79	0.91	15.74	0.92	0.80	1.03	$16^h53^m54.35^s$	$+61^o27'29.67"$
$PRHB165356+612642$	15.88	1.43	15.87	1.41	1.15	1.53	$16^h53^m54.99^s$	$+61^o26'41.26"$
$PRHB165406+612615$	16.22	0.90	16.16	0.85	0.34	1.02	$16^h54^m05.65^s$	$+61^o26'14.39"$
$PRHB165405+612546$	17.34	0.91	17.31	0.82	0.31	1.12	$16^h54^m03.86^s$	$+61^o25'45.04"$
$PRHB165349+612529$	...	...	14.24	0.60	0.05	0.83	$16^h53^m49.74^s$	$+61^o25'29.53"$
$PRHB165428+612516$	15.91	0.89	15.85	0.90	0.48	1.04	$16^h54^m27.22^s$	$+61^o25'14.83"$
$PRHB165436+612419$	15.69	0.85	15.64	0.82	0.31	0.94	$16^h54^m35.52^s$	$+61^o24'18.36"$

References

Andreazza C.M., Vilas-Boas J.W.S., 1996, A&AS 116, 21
Bahcall J.N., 1986, ARA&A 24, 577
Bahcall J.N., Soneira R.M., 1980, ApJS 44, 73
Burrows D.N., Mendenhall J.A., 1991, Nat 351, 629
Cardelli J.A., Clayton G.C., Mathis J.S., 1989, ApJ 345, 245
Gladders M.D., Clarke T.E., Burns C.R., et al., 1998, ApJ 507, L161
Goerigk W., Mebold U., Reif K., Kalberla P.M.W., Venden L., 1983, A&A 120, 63
Goerigk W., Mebold U., 1986, A&A 162, 279
Grebel E.K., Richtler T., de Boer K.S., 1992, A&A 254, L5
Herbstmeier U., Mebold U., Snowden S.L., et al., 1995, A&A 298, 606
Jacoby G.H., Hunter D.A., Christian C.A., 1984, ApJS 56, 257
Landolt A.U., 1992, AJ 104, 340
Lillenthal D., Wennmacher A., Herbstmeier U., Mebold U., 1991, A&A 250, 150
Magnani L., de Vries C.P., 1986, A&A 168, 271
Mebold U., Cernicharo J., Velden L., et al., 1985, A&A 151, 427
Mihalas, D., Binney, J., 1981, Galactic Astronomy – Structure and Kinematics, Second Edition (Freeman: San Francisco)
Odenwald S.F., Rickard L.J., 1987, ApJ 318, 702
Snowden S.L., Mebold U., Hirth W., Herbstmeier U., Schmitt J.H.M., 1991, Sci 252, 1529
Thoraval S., Boisse P., Duvert G., 1997, A&A 319, 948
Wheelock S.L., Gautier T.N., Chillemi J., et al., 1994, In: The IRAS Explanitory Supplement. NASA report N95-22539